



# ENHANCING DECONVOLUTION WITH FUNCTIONAL BEAMFORMING

Robert P. Dougherty<sup>1</sup>

<sup>1</sup>OptiNav, Inc.

1414 127<sup>th</sup> PL NE #106, 98005, Bellevue, WA, USA

## ABSTRACT

Beamforming deconvolution is modified to use the output of Functional Beamforming as the dirty map and to change the elements of the point spread function, raising them to the power  $\nu$ . The first change increases the dynamic range of the method. The second improves the condition of the system of equations to be solved, possibly speeding convergence. It also provides a difficulty in that the modelled resolution is higher than FB can really provide. The algorithm modifications are described and sample results are given for a warehouse test with a fan and a loudspeaker and array benchmark dataset DLR 1. The process applies to various forms of DAMAS including the original, DAMAS2, NNLS and linear programming. The interaction with CLEAN/CLEAN-SC has yet to be explored. Robust Functional Beamforming can be applied to counter the effects of peak loss in FB due to steering vector errors.

## 1 INTRODUCTION

DAMAS and similar deconvolution methods are powerful but can be tricky because rejection of interference from sources outside the grid is weak, convergence can be slow, and the final solution can have unphysical arrangements of dots. Poor exclusion of interference reduces the dynamic range, potentially concealing weak sources. Slow convergence raises a barrier to use of the method due to a need for elaborate computer resources. Unphysical deconvolved maps degrade confidence in the method. The problems, like many aspects of deconvolution, are related to the Point Spread Function (PSF). Reality of array design, finite size, defined shape, and sparse aperture sampling, creates PSFs with many sidelobes at high frequency and excessive width at low frequency. These decrease the dynamic range of the resulting integrated spectra.

Functional Beamforming (FB) [1-4] considerably improves the dynamic range of beamform maps, but does not directly offer the quantitative nature or high resolution of deconvolved maps. In considering FB with index  $\nu$  for a single source of interest and a single

source of interference, application of the Löwner-Heinz inequality shows that the PSF for this pair of points is effectively raised to the power  $\nu$ . This provides the dynamic range improvement because a typical sidelobe height of, say 0.1, with, say,  $\nu = 20$ , results in final sidelobe effect of 1.E-20, or -200 dB.

It has recently been observed [5] that the expression for the relationship between the FB output and the strengths of multiple sources can be represented by a model that is very similar to the source-receiver model of DAMAS and other deconvolution methods. This is outlined below after first reviewing DAMAS.

In the DAMAS model, the beamform output at (beamform map) location  $i$  is given by a weighted sum of the strengths the other sources, where source  $j$  enters with a weight factor of the PSF,  $A_{ij}$ . Assuming that all of the (mutually incoherent) sources contributing to the beamforming value are located in the beamform grid, the beamform map value at point  $i$  is given by

$$b(\mathbf{g}_i) \approx \sum_{j=1}^M A_{ij} s_j \quad (1)$$

The deconvolution problem is to solve Eq. (1) for the  $M$  unknown source strengths  $s_j$  given (usually)  $M$  beamform values  $b(\mathbf{g}_i)$  and known PSF values. It is a physical constraint that  $s_j \geq 0$ . The method of solution, in a least-squares sense, can be the original DAMAS [6], or any number of variations such as Non-Negative Least Squares (NNLS) [7].

Equation (1) is an approximation because there may be sources located off the grid. It really should be written as an inequality

$$b(\mathbf{g}_i) \geq \sum_{j=1}^M A_{ij} s_j \quad (2)$$

This inequality can be derived from the non-negative nature of the total cross spectral matrix (CSM)  $\mathbf{C}$  and the component CSMs of any of the contributing sources, together with the beamforming formula

$$b(\mathbf{g}_i) = \mathbf{g}_i' \mathbf{C} \mathbf{g}_i \quad (3)$$

Here the steering vectors  $\mathbf{g}_i$  are vectors of Green's functions, normalized to unity. Beamforming values such as Eq. (3) are conveniently normalized to the scale of individual array microphones by dividing by the number of microphones,  $N$ . This notation is tedious, and is omitted here. As shown, Eq. (3) can be interpreted as an estimate of the total power the array from source  $i$ .

The philosophy of deconvolution can be viewed as hoping that Eq. (2) is not a very strong inequality, solving it as if it were an approximation, and understanding that the resulting  $s_j$  may be overestimates.

The FB expression is steering vector  $\mathbf{g}_i$  is

$$b_\nu(\mathbf{g}_i) = \left[ \mathbf{g}'_i \mathbf{C}^{\frac{1}{\nu}} \mathbf{g}_i \right]^\nu \quad (4)$$

By using the operator concavity of the function  $f(t) = t^{\frac{1}{\nu}}$  for  $\nu \geq 1$  it is proven in [5] that

$$b_\nu(\mathbf{g}_i) \geq \sum_{j=1}^M A_{ij}^\nu s_j \quad (5)$$

This suggests solving Ineq. (5) as if it were an equality using DAMAS or NNLS, with the input beamforming values replaced by the FB values and the PSF elements raised to the power  $\nu$ . It is also possible to solve it as an inequality, giving a generalization of the linear programming beamforming method [5,8]. This is called Functional Beamforming Linear Programming (FBLP).

Two big effects of  $\nu$  are to 1) remove much of the interference from the beamforming values on the RHS of (5) due to the power of FB and 2), make the system of linear equations to be solved in the deconvolution much better conditioned and simpler to solve.

If a matrix version of Ineq. (5) is desired, it would be

$$\vec{b}_\nu \geq A^{\circ \nu} \vec{x} \quad (6)$$

where  $\vec{b}_\nu = [b_\nu(\mathbf{g}_1), \dots, b_\nu(\mathbf{g}_N)]^T$ ,  $\vec{x} = [s_1, \dots, s_M]^T$ ,  $A$  is the usual PSF matrix, and  $\circ \nu$  refers to the Hadamard power. This is different from the operator power that appears in Eq. (4).

The operation  $\circ \nu$  improves the condition of  $A$  because, in this setup ( $A_{ij} = |\mathbf{g}'_i \mathbf{g}_j|^2$ ), the diagonal elements of  $A$  are unity and not affected by  $\circ \nu$ , and the off-diagonal elements are between 0 and 1 and are made smaller by  $\circ \nu$ .

The peak loss of FB from inaccurate steering vectors can be countered with Robust Functional Beamforming (RFB) [9]. This method adjusts the steering vector by applying one step of method of steepest ascent to increase the beamforming result. A trust region with a radius of  $\epsilon$  limits the length of the step. Specification of  $\epsilon$  is an input to the method.

## 2 FAN-SPEAKER EXAMPLE

A 30 cm, 40 element acoustic camera was used to image 2-foot duct containing a fan and a loudspeaker as shown in Figs. 1d) and 2d). The data were first processed by making 1/12 octave band DAMAS deconvolution images of the whole field of view of the acoustic camera using  $\epsilon = 0$  and  $\nu = 1, 2$  & 8. Sample images for 3 kHz and 16 kHz are shown in Figs. 1 & 2 respectively. Increasing  $\nu$  improves the resolution of the deconvolved image.

ROIs for the fan and speaker sources were defined and the component spectra were computed by integration. The results are shown in Fig. 3 a)-c). Figure 3 d) gives the array median spectra for the fan and the speaker operating separately. These are the expected results for deconvolution spectra. It can be seen that increasing  $\nu$  increases the low frequency performance of the deconvolution for the speaker. At low frequency the array resolution is challenged and the fan interferes strongly with the speaker noise.

Figure 4 compares the integrated FBLP, DAMAS, and NNLS spectra for the fan with the expected result. As  $\nu$  increases, the deconvolution values increase above the correct result.

This is a result of the PSF in Eq. (5) or (6) being sharper than the actual resolution of FB [9]. This difficulty is an outstanding problem for the FB-deconvolution concept. In the case of FBLP, one solution is to thin the grid points in the ROI to remove elements of the PSF with values above a threshold [9]. Part b) of Fig. 4 show that PSF thinning resolves the problem in this case. Figure 5 gives another example, this time using the speaker source. In Fig 4a), with no thinning, it is seen that a large value of  $\nu$  lead to both undershoot and overshoot. Applying RFB with  $\epsilon = 0.2$  makes the overshoot stronger. Part b) shows that PSF thinning resolves the problem. Note that peak loss does not occur in case of  $\nu = 80$ ,  $\epsilon = 0.$ , where it might be expected. This is attributed to the fact that the speaker is a reasonably simple source with a well-known steering vector.

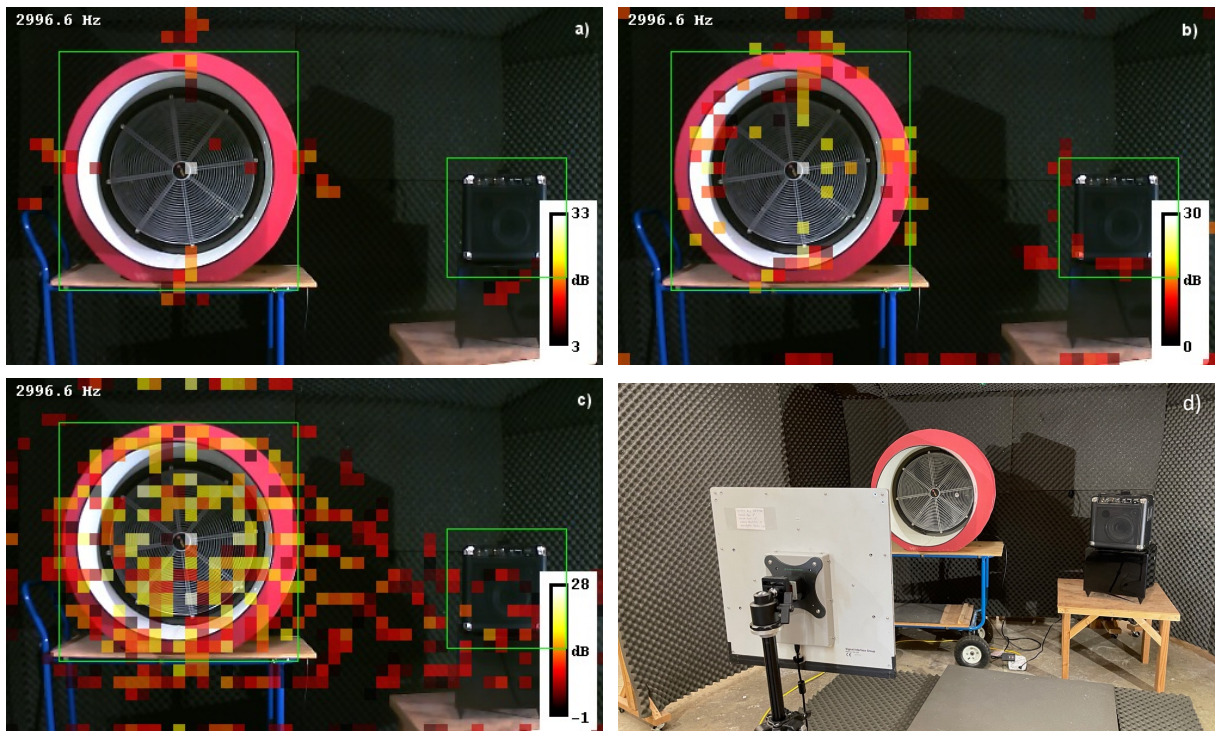


Fig. 1 DAMAS deconvolution at 3 kHz,  $\epsilon = 0$ . a)  $\nu = 1$  b)  $\nu = 2$ , c),  $\nu = 8$ , d) photo.

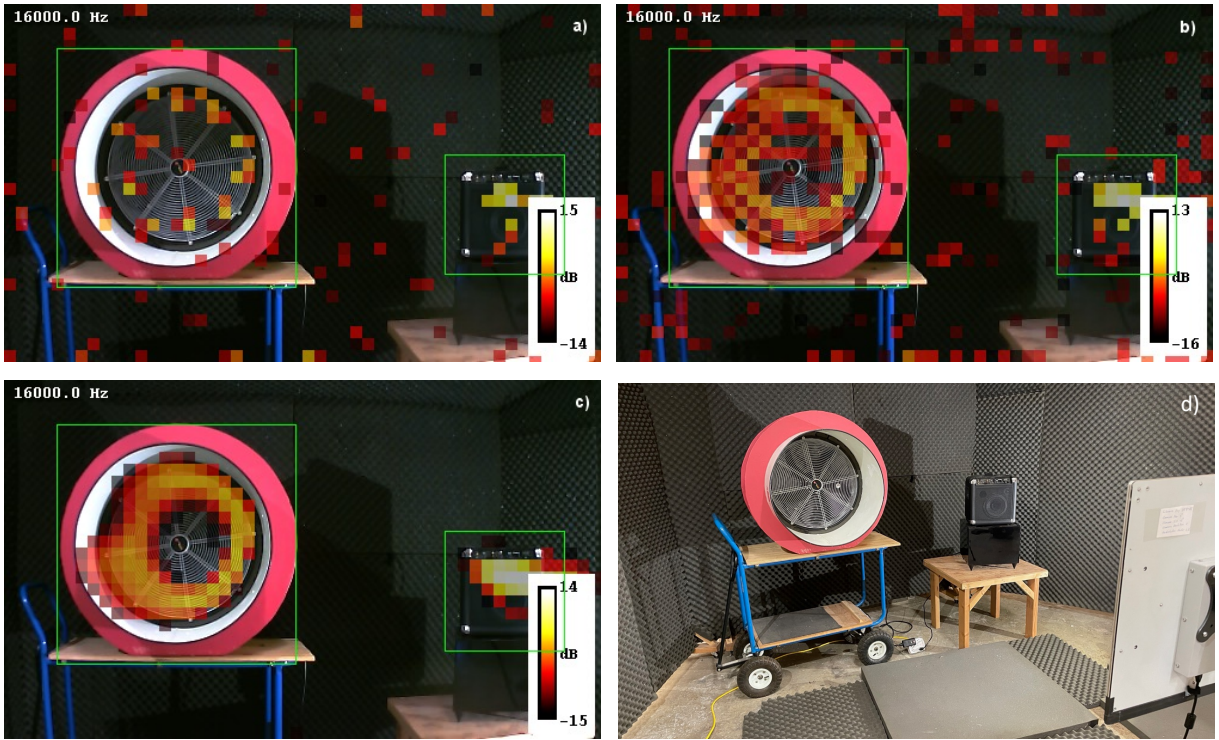


Fig. 2 DAMAS deconvolution at 16 kHz,  $\epsilon = 0$ . a)  $\nu = 1$  b)  $\nu = 2$ , c),  $\nu = 8$ , d) photo.

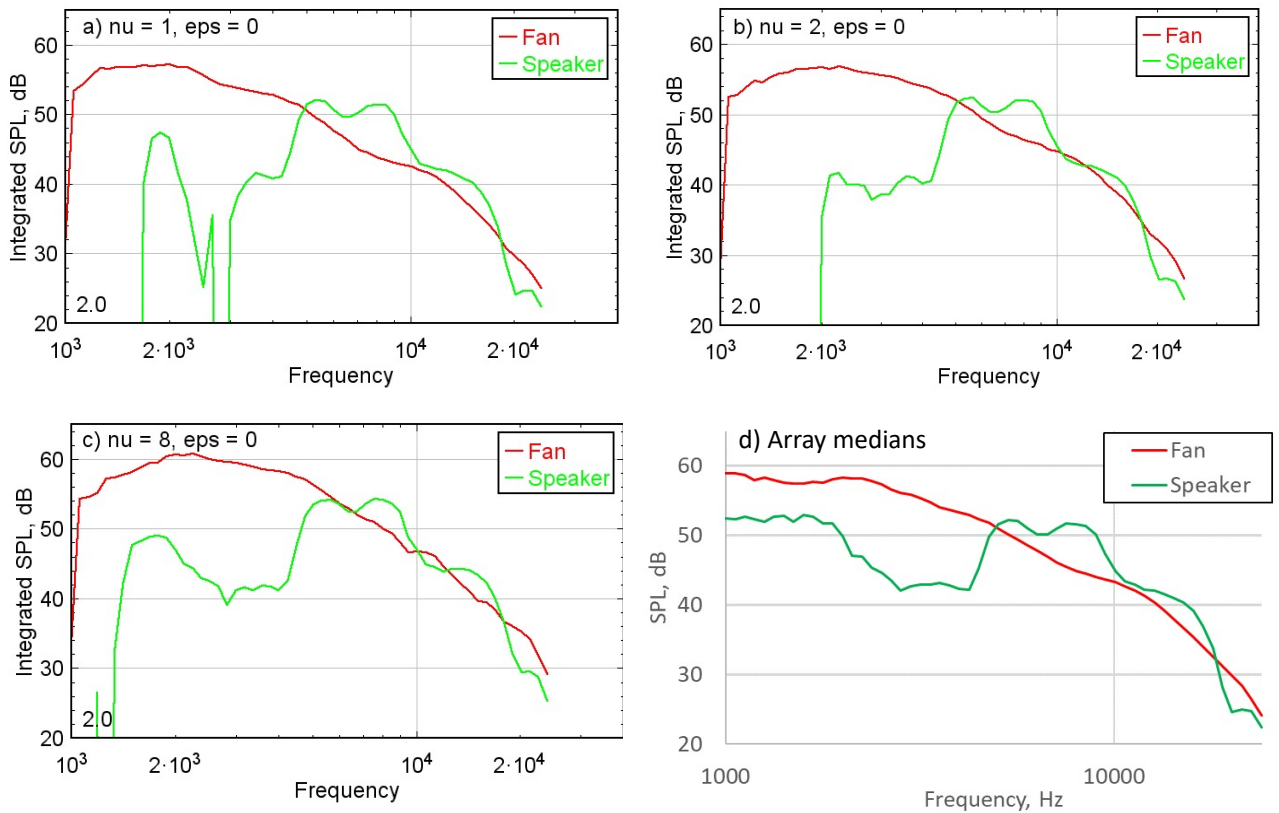


Fig. 3 Integrated spectra from DAMAS deconvolution.

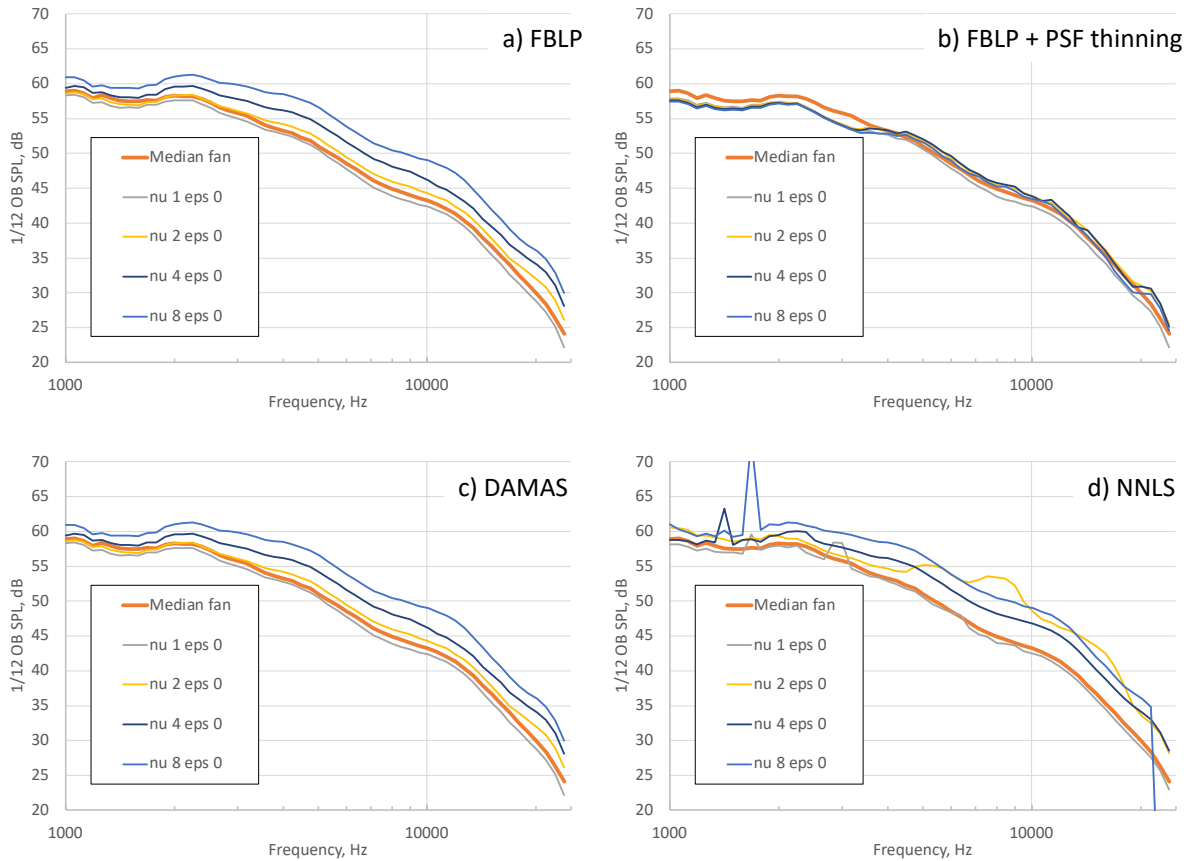


Fig. 4 Deconvolution spectra for the fan alone.  $\epsilon = 0$ . a) FBLP, b) FBLP with PSF thinning ( $t = 0.3$ ), c) DAMAS, d) NNLS.

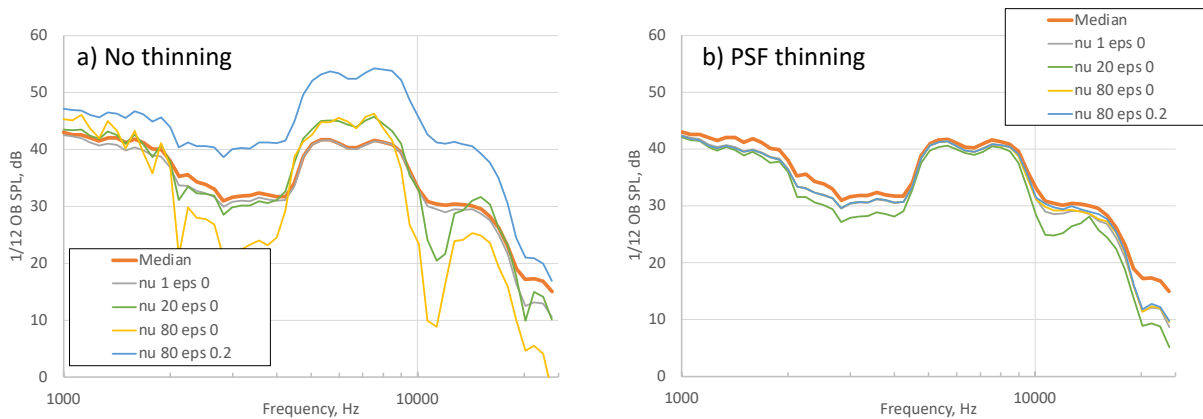


Fig. 5 FBLP Deconvolution spectra for the speaker source with and without PSF thinning.

### 3 BENCHMARK DLR 1 EXAMPLE

Array Methods Experimental Benchmark dataset DLR 1 is a Donrrier-728 semi span model tested in the high lift configuration in the DLR-Cologne site [10]. The experimental data for the following results were downloaded from the Benchmark data repository [11]. The test setup in shown in Fig. 6.

The array data from the benchmark files had 135 microphones. The case analyzed was run 59, with an angle of attack of  $3^\circ$  and a Mach number of 0.25. A dead microphone, channel 41, was removed, leaving 134. Binary array shading was applied by excluding microphones with  $kr > 100$ , where  $k$  is the wavenumber and  $r$  is the radial distance of the microphone from the array center in the plane of the array.

In the iterative results shown, 100 iterations were used. Testing increased numbers of iterations produced very small changes in the results. In the case of NNLS, if the residual stopped changing then the iteration terminated early.

Exploratory runs of several methods with at 1992 Hz and 8496 Hz with a 1.0 cm grid (15,476 points) and no binning were performed. The results are shown in Figs. 6&7, respectively.

The final beamforming grid was a 0.5-cm with  $212 \times 292$  points. For deconvolution,  $4 \times 4$  binning was performed, giving a grid of 3,869 points. The ROIs are given in Fig. 9. Two runs of DAMAS deconvolution were performed. The first case was conventional DAMAS:  $\nu = 1$ ,  $\epsilon = 0$ . Boundary layer noise on the diagonal of the CSM was handled by setting the diagonal elements to 0, performing an eigenvalue decomposition, adding a constant to all of the eigenvalues to adjust the eigenvalue  $1/3$  from the small end of the list to 0, and finally replacing any negative eigenvalues by a small positive value.

The second run was DAMAS with the same diagonal treatment, but  $\nu = 8$  and  $\epsilon = 0.2$ .

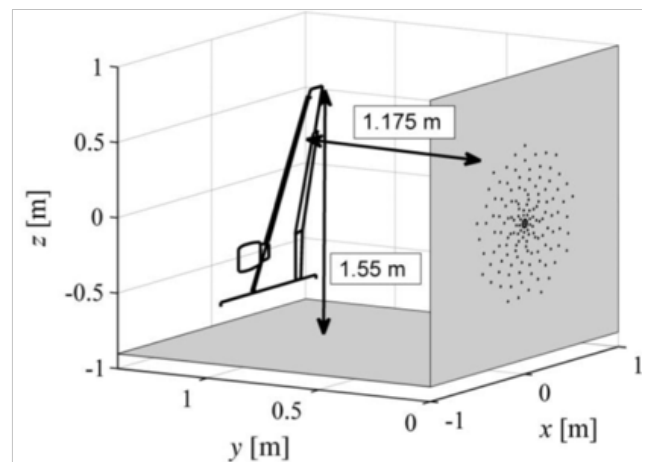
Sample deconvolved maps are shown in Fig. 10, where the top row is conventional DAMAS and the bottom row include the FB modifications. The use of FB substantially improves the appearance of the results.

The integrated spectra are shown in Fig. 11. An increase in dynamic range for the FB case is evident.

For comparison, the results of FDLP from [5] are shown in Fig. 12. This calculation used FBLP for the individual ROIs with  $\nu = 80$ ,  $\epsilon = 0.2$ , and PSF thinning with  $t = 0.3$ . The ROIs used in [5] are the same as the ones here, except that [5] excluded the inboard flap track. The spectra appear similar.



Fig. 6 Setup for Benchmark DLR 1, from Ref. 11.



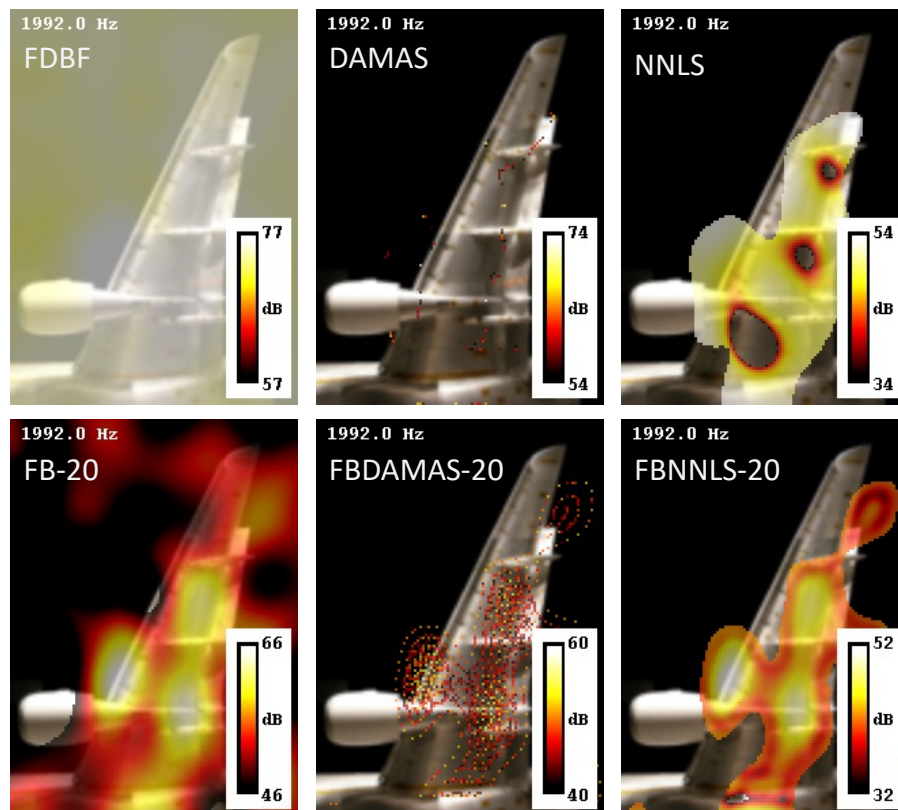


Fig. 7 Beamforming plots for DLR 1 for 1992 Hz using  $\epsilon = 0$ .

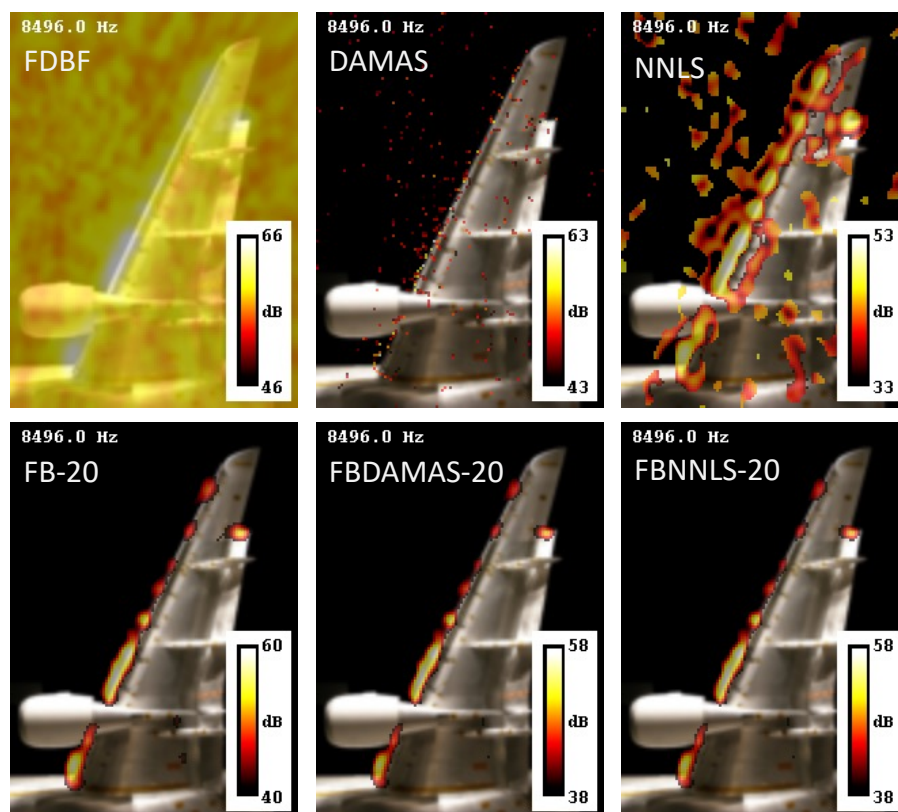


Fig. 8 Beamforming plots for DLR 1 for 8496 Hz using  $\epsilon = 0$ .

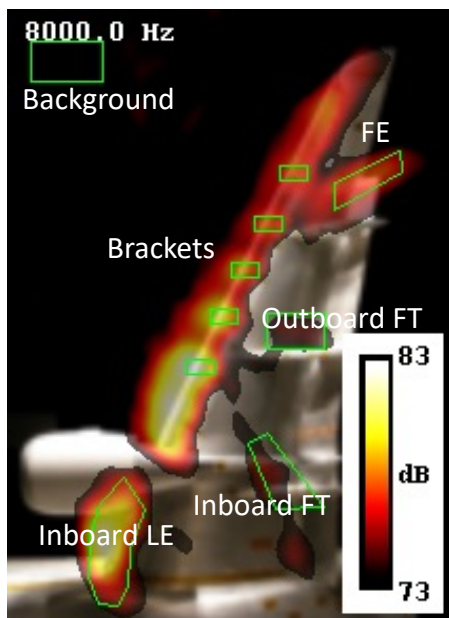


Fig.9. Regions of interest for DLR 1. RFB with  $\nu=20$ ,  $\epsilon=0.2$ .

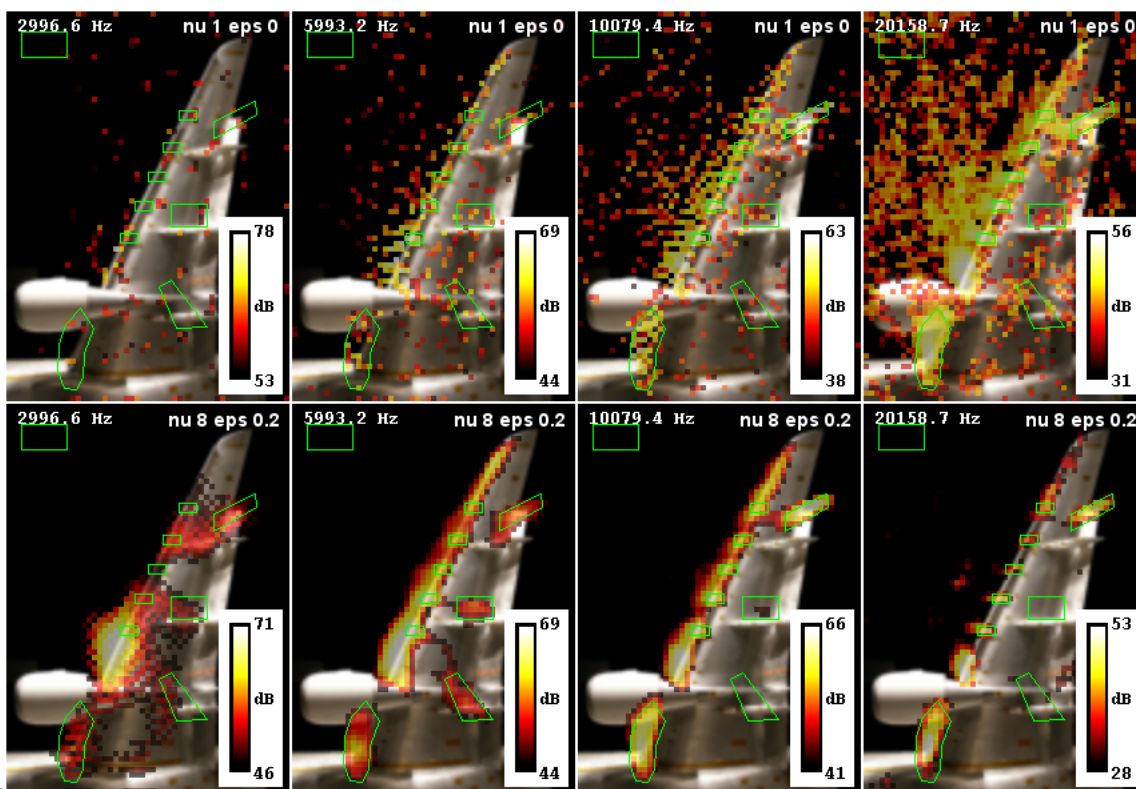


Fig.10. DAMAS deconvolution for DLR 1. Top row:  $\nu=1$ ,  $\epsilon=0$ . Bottom row:  $\nu=8$ ,  $\epsilon=0.2$ .

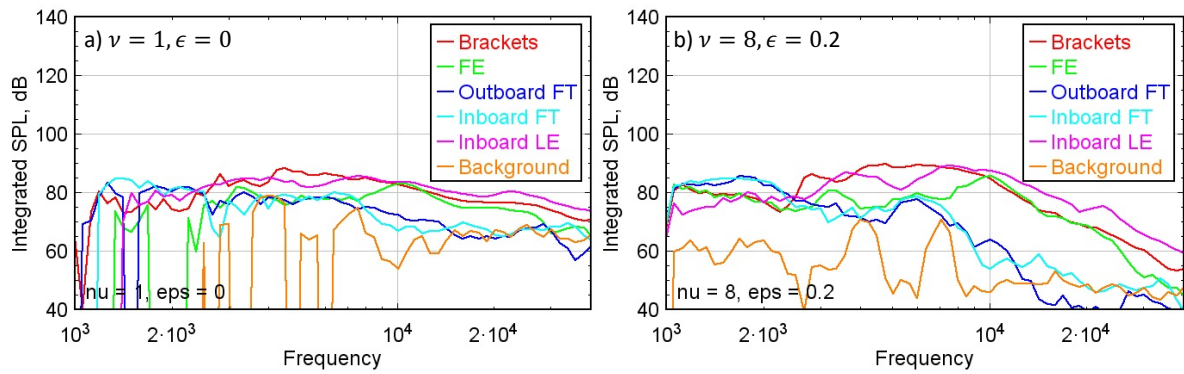


Fig. 11. Integrated DAMAS deconvolution for DLR 1. a)  $\nu = 1, \epsilon = 0$ , b)  $\nu = 8, \epsilon = 0.2$ .

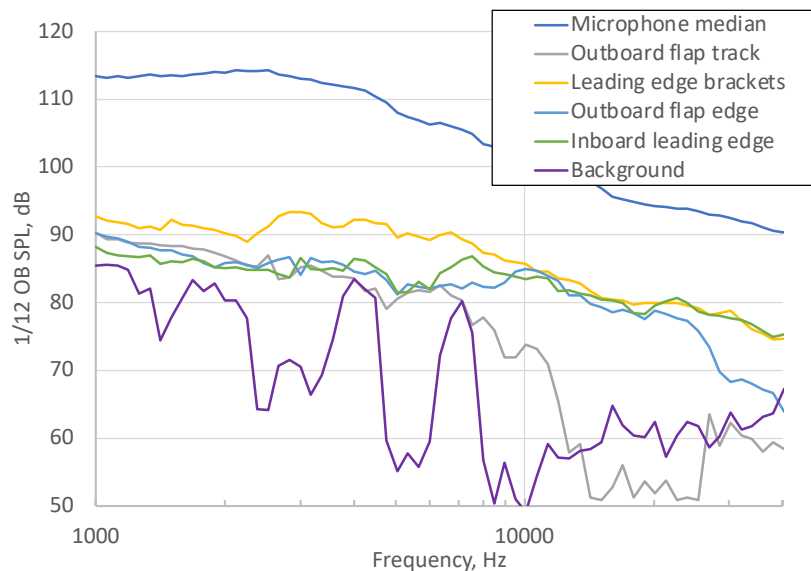


Fig. 12. FBLP plot from [5] for the DLR 1.  $\nu = 80, \epsilon = 0.2, \text{PSF thinning } t = 0.3$ .

## 4 CONCLUSIONS

Altering deconvolution by incorporating Functional Beamforming significantly increases the dynamic range of the results. Quantitative results are improved by using Robust Functional Beamforming. Work remains to find a way to compensate for an increase in levels resulting from an overoptimistic expression for the point spread function.

## REFERENCES

- [1] Merino-Martinez, R. G. Herold, M. Snellen, and R. P. Dougherty, “Assessment and comparison of the performance of functional projection beamforming for aeroacoustic measurements”, BeBeC 2020-S7.
- [2] Merino-Martinez, R, M. Snellen and D.G. Simmons, “Functional Beamforming Applied to Full Scale Landing Aircraft”, BeBeC-2016-D12.
- [3] Dougherty, R.P., “Functional Beamforming”, Berlin Beamforming Conference, BeBeC 2014-1, 2014.

- [4] Dougherty, R.P., "Functional Beamforming for aeroacoustic source distributions", AIAA Paper 2014-3066, 2014.
- [5] Dougherty, R.P., "Functional Beamforming Linear Programming for Determining Aeroacoustic Component Spectra", Submitted for the 28th AIAA/CEAS Aeroacoustics Conference, June, 2022.
- [6] Brooks, T.F., and W.M. Humphreys, "A deconvolution approach for the mapping of acoustic sources (DAMAS) determined from phased microphone arrays. *J. Sound Vib.* 294(4–5), 856–879 (2006).
- [7] Ehrenfried K, Koop L. Comparison of iterative deconvolution algorithms for the mapping of acoustic sources. *AIAA journal.* 2007 Jul;45(7):1584-95.
- [8] Dougherty, R.P., Ramachandran and G. Raman "Deconvolution of Sources in Aeroacoustic Images from Phased Microphone Arrays Using Linear Programming," R.P., AIAA Paper 2013-2210, Berlin, Germany, 2013.
- [9] Dougherty, R.P. "Robust Functional Beamforming", Proc 9th Berlin Beamforming Conference; June 9-10, 2022, Berlin, Germany, 2022, Paper no. BeBeC-2022-S7.
- [10] Bahr, C.J., W.M. Humphreys, D. Ernst, T. Ahlefeldt, C. Spehr, Q. Leclère, C. Picard, R. Porteous, D. Moreau, J.R. Fischer, and C. Doolan, "A Comparison of Microphone Phased Array Methods Applied to the Study of Airframe Noise in Wind Tunnel Testing," AIAA Paper 2017-3718.
- [11] Ahlefeldt, T., "Array Methods HDF5-Benchmark data" Downloaded from <https://www.b-tu.de/fg-akustik/cloud/> maintained by Thomas Geyer, January, 2020.